Jet-flap installation noise of pylon mounted jet engine on 3D wing

Christian Jente *
German Aerospace Center (DLR), Braunschweig, Germany

Jérôme Huber † and Florian Renard ‡
Airbus Operations SAS, Toulouse, France

Tristan Goffredi§ and Edoardo Paladini¶
Safran Aircraft Engines, Moissy Cramayel, France

The cost of experimental testing allows to focus only on a finite number of operations for installation noise. How can other operations be interpolated in between test conditions? How can test points with partially poor signal to noise ratio be repaired? How is it possible to extrapolate to and cross-compare with a known test point which is out of scope for the current test facility, but has been measured before in another wind tunnel? All of the above can be attempted with the knowledge of the problem-specific physics, which is among others represented in terms of velocity scaling laws.

Hence, a major contribution presented in this paper is the analytical derivation of an analogy for the far-field noise of installed flight jets and a cross-check with experimental data from the DJINN AWB test. This analogy is a specific solution of Ffowcs-Williams-Hawking's and Curle's analogies for fixed objects which experience unsteady flow fluctuations on their surfaces.

The analysis shows that velocity scaling exponents are qualitatively different depending on directivity, mainly between forward and rear arc. The experimentally acquired *isolated* flight jet noise data scales with $I \propto \Delta U^6 U_c^2$ in the forward arc and with $I \propto \Delta U^8$ in the rear arc. *Installed* flight jets are dominated by loading noise $I \propto \Delta U^6$ in the forward arc, and are otherwise very similar to jet noise, i.e. in the rear arc they scale with $I \propto \Delta U^8$.

The transition of velocity scaling coefficients between forward arc and rear arc are extracted by a study over 47 flyover microphones using various operations of either same shear layer difference velocity or same shear layer convection velocity. The exponents can also be used to improve the prediction of extrapolating to out-of-scope wind tunnel velocities.

This is showcased in a case study, where a test point with wind tunnel velocity of 60 m/s needs to be predicted with a maximally available wind tunnel speed of 40 m/s. The conventional method of using the same velocity difference velocity delivers nearly the same OASPL (±0.3 dB), good accuracy in the rear arc and causes deviations in the shape of the third-octave band spectrum by ±2 dB - mainly in the forward arc. The new method proposes to scale a same shear layer convection velocity datapoint. This delivers the same accuracy in OASPL, but the third-octave band spectrum deviates by only ±1 dB around the reference.

What is the transferability to other related problems, e.g. the often tested freely positioned engine integrations without any pylon? A cross-comparison with the DJINN-JExTRA experiment shows that the velocity scaling coefficients are comparable, as long as tonal components are removed from the spectra. Another takeaway is the acoustic importance of the pylon and the necessity to include it in the aero-geometric characterization of the physical problem.

*Technical Acoustics TEA, christian.jente@dlr.de
†Aeroacoustic Sources, jerome.huber@airbus.com
‡Aeroacoustic Sources, florian.renard@airbus.com
§Aeroacoustic Engineer, tristan.goffredi@safrangroup.com
¶Aeroacoustic Engineer, edoardo.paladini@safrangroup.com

I. Introduction

VARIOUS velocity scaling coefficients for jet installation noise were reported in the past, most of them fall into the range of 5 (trailing edge noise) to 6 (lift fluctuation noise), e.g. 5.3 by Sengupta [1, Fig. 14]. Higher coefficients close to 7 have also been presented, e.g. by Azarpeyvand [2]. Why are these exponents different? And how can the knowledge about the exponents be applied to solve relevant challenges? These questions will be attempted to be answered in this paper.

The scientific backbone of finding a suitable velocity scaling candidate is to test out different characteristic jet shear layer properties. The commonly used jet shear layer characterization refers to the axisymmetric properties of the aerodynamic far-field (or ➡ fully developed region, see Fig. 1) where peak jet noise is located.

But, the flap trailing edge is typically positioned in the ➡ initial merging zone of the jet. Therefore, the approach is to investigate the problem through the eyes of the so-called aerodynamic near-field shear layer: a thin mixing layer that originates at the nozzle lip of an single-stream nozzle and that "fuels" the far-field shear layer downstream the ending jet's potential core. Any references to the jet shear layer typically refer to the near field shear layer in this paper.

Lip line properties have been measured by many authors, i.a. Bridges and Wernet [3, Figs. 17 and 19, bottom left]. The most important property is the axial mean velocity U_c at the lip line which is remarkably constant within the initial merging zone (Jente and Delfs [4, pp. 3-8]). The relevance of fine scale turbulences from the near field shear layer towards forward arc jet noise has been documented by Tam et al. [5] [6]).

	aerodynamic near-field	**aerodynamic far-field**
	initial merging region	fully-developed / self-similarity region
S/L origin	nozzle lip ($x \approx 0$, $r = D_j/2$) / mixed jet radius	engine axis ($x < 0$, $r = 0$) / jet centerline
characteristic velocity	nozzle lip velocity $U_c = U(r = D_j/2)$ nearly constant in streamwise direction	e.g. centerline velocity $U(r = 0)$ (declines in streamwise direction [7])

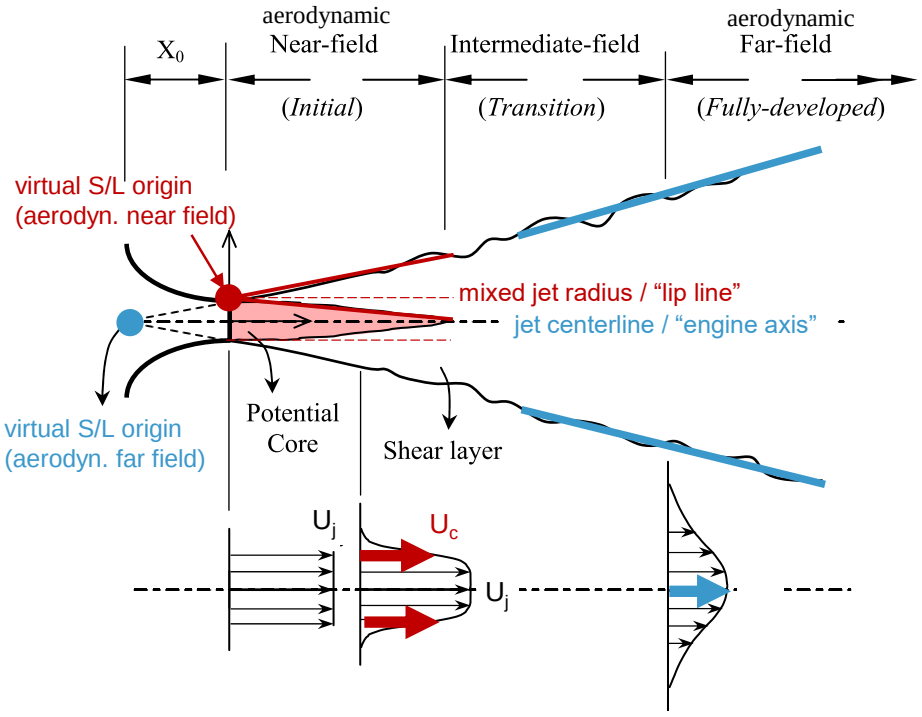

Fig. 1 Characteristic jet shear layer properties, illustrated for an idealized single stream jet. Image adapted from Abdel-Rahman [8, Fig. 1]

Nomenclature

α	=	shear layer convection coefficient, *here:* $\alpha = 0.64$
Δf	=	bandwidth of narrowband frequencies
ΔU	=	shear layer difference velocity
$\Delta X, \Delta Y, \Delta Z$	=	test section dimension
δ_F	=	flap deflection angle
δ_ω	=	shear layer width
γ	=	adiabatic index
λ	=	wave length
ρ_∞	=	(static) density of medium in acoustic room
ρ_j	=	static density of jet
$\boldsymbol{\tau}$	=	viscous stress tensor
θ	=	polar angle of microphone, from engine exhaust (aft-front)
A	=	area, e.g. bypass outlet area
a_j	=	local speed of sound in jet medium
a_∞	=	speed of sound in acoustic room
c	=	chord length
D_{mix}	=	mixed jet diameter
$\boldsymbol{e}$	=	unity vector
$\boldsymbol{F}$	=	aerodynamic force (vector)
f	=	frequency
f_c	=	characteristic frequency
H	=	engine integration height
He	=	Helmholtz number
I	=	sound intensity
$\boldsymbol{I}$	=	identity matrix
L	=	engine integration length
L_0	=	characteristic length
M_{ac}	=	acoustic Mach number
M_j	=	jet Mach number
m, n, q	=	velocity scaling coefficients
$\boldsymbol{n}$	=	normal vector
p'	=	sound pressure
p_∞	=	(static) ambient pressure of acoustic room
r_U	=	velocity ratio between wind tunnel and jet velocity
R	=	distance oberver to engine axis
r_0	=	distance source-observer
R_{mix}	=	mixed jet radius
SPL	=	sound pressure level
S	=	(surface) area
Sr	=	Strouhal number
$\boldsymbol{T}$	=	Lighthill's stress tensor
TTR	=	Total temperature ratio between jet and test room
t	=	time
U_c	=	shear layer convection velocity
U_j	=	jet velocity
V	=	volume
v'	=	acoustic particle velocity
x, y, z	=	coordinates
$x_{0,NF}$	=	virtual origin of near field shear layer
$\mathcal{F}$	=	dimensionless flight operations factor
$\mathcal{G}$	=	dimensionless geometry factor
$\mathcal{T}$	=	dimensionless temperature factor
:	=	double contraction
AWB	=	Aeroacoustic Wind tunnel Braunschweig, a DLR test facility
JExTRA	=	Jet noise experiments at AT-TRA, a DLR test facility
S/L	=	shear layer
UHBR	=	Ultra High Bypass Ratio
w.r.t.	=	with respect to

II. Experiment

Experimental data was gathered at the Aeroacoustic Wind tunnel Braunschweig [9] (AWB), a DLR test facility in Northern Germany (see Fig. 3). AWB is a closed-circuit wind tunnel with a rectangular wind tunnel nozzle ($\Delta Y = 0.8\,\mathrm{m} \times \Delta Z = 1.2\,\mathrm{m}$), an open test section ($\Delta X = 3.6\,\mathrm{m}$) and wind tunnel velocities of up to 60 m/s.

The SAFRAN engine model is a dual stream short cowl UHBR engine with a bypass-to-core area ratio in the order of 7, and a mixed* jet diameter D_{mix} close to 100 mm. Bypass and core engine were operated at equal velocity, achieving several same speed jet operations in between $145 - 295\,\mathrm{m/s}$ (see Fig. 2). The temperature behaviour of the wind tunnel allows for cold / unheated ambient air tests, i.e. the total temperature ratio between jet and test room $TTR = \frac{291\,\mathrm{K}}{296\,\mathrm{K}} \approx 0.98$ is very close to unity.

The AIRBUS RDJ80-wing is a right-hand (starboard-side) half model with a chord length of 300 mm in the engine integration plane. The two-element wing consists of its main wing and the flap which are both tripped on pressure side and suction side. The flap deflection angle is fixed to $\delta_F = 14\,°$.

The engine is integrated under the wing via a pylon model. The presence of the pylon decreases the bypass outlet area and causes asymmetry in the jet.

The engine integration length between bypass nozzle outlet and flap trailing edge is $L = 2.77 D_{mix}$. The two engine integration heights are $H_1 \approx 0.98 D_{mix}$ and $H_2 \approx 0.71 D_{mix}$.

Operational parameters of the test campaign are defined by wind tunnel velocity U_∞ and jet velocity U_j and displayed in Fig. 2.

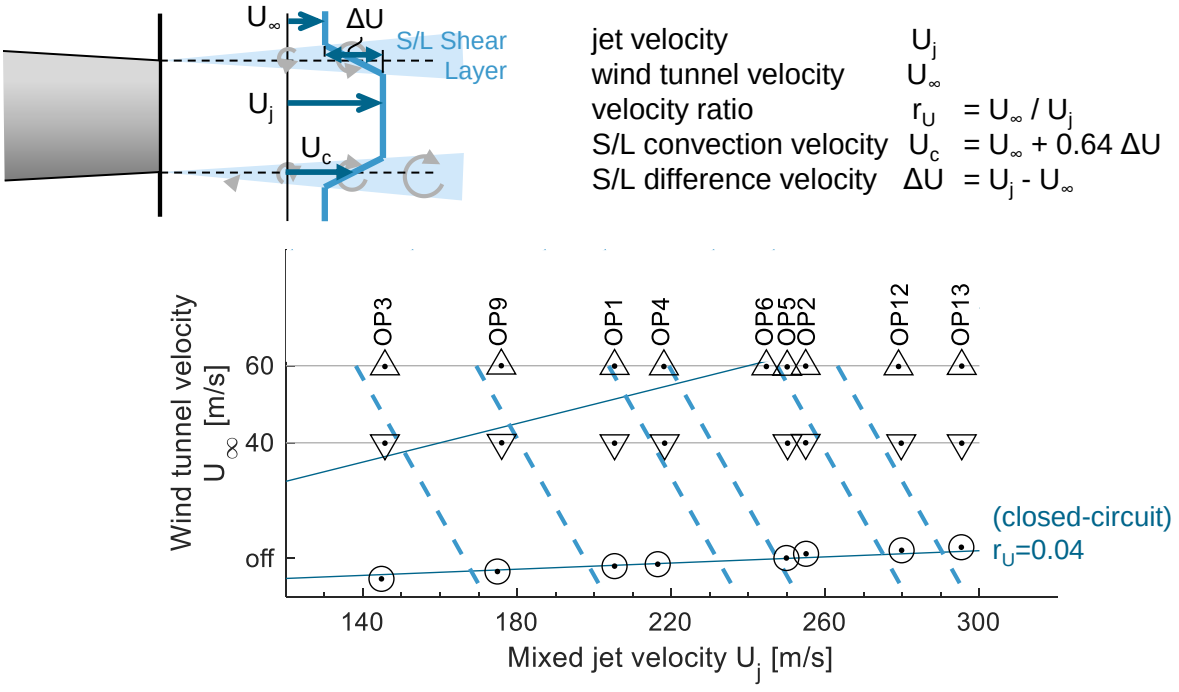

Fig. 2 Wind tunnel test operations with the following markers by wind tunnel velocity: ◯ circle/zero = wind tunnel off, △ triangle pointing upwards = higher wind tunnel setting of 60 m/s, ▽ triangle pointing downwards = lower wind tunnel setting of 40 m/s. Iso-contours for the following *near field* shear layer properties: constant velocity ratio r_U (— solid line), and shear layer convection velocity U_c (- - - dashed line)

*Fully-mixed jet variables are considered as defined by the SAE ARP 876 norm.

III. Acoustic instrumentation and data processing

Instrumentation The flyover arc under the model is instrumented with a DLR Berlin line array (see Fig. 3). The distance between the engine axis and the line array is $R = 1.78$ m, which is a rather close [10, p. 203] geometric distance ($R/D_{mix} = 17.8$) for jet-related problems. The polar arc is resolved by 47× ¼" MK301 free-field microphones (Microtech Gefell) in between aft-to-front installation angles of 50° to 134° w.r.t. x = flap trailing edge and z = engine axis (see top of Fig. 4).

Data processing 10 Hz narrowband and third-octave sound pressure level has been normalized to same propagation distances using the following measurement reference points:

- $x = 7D_{mix}$ and z = engine axis: for isolated jet noise
- x = flap trailing edge and z = engine axis: for installed jet noise.

The presented acoustic data is corrected for microphone characteristics[11], shear layer refraction (Amiet [12]), and atmospheric absorption (Bass et al. [13], which is also ISO 9613 [14]).

IV. Velocity scaling exponents along the flyover arc

A. The systematic difference between forward and rear arc

Depending on directivity, *installed jets* produce either very similar gains as the Lighthill's power 8 jet noise (i.e. in the rear arc), or produce higher gains and other velocity scaling exponents than jet noise (i.e. in the forward arc). This forward arc excess noise is mainly produced by jet-flap interaction, and the low-frequency component can be interpreted as loading noise $I_{loading} \propto (\Delta U)^6$ (see derivation in appendix VII).

Lighthill's power 8 jet noise, if taylored for flight operations of the *isolated jet*, scales with $I_{jet} \propto (\Delta U)^8$ in the rear arc, yet collapses differently in the forward arc. This effect was reported by several authors, i.a. Michalke and Michel [15], Tam et al. [5]. The AWB data scales well with $I_{jet} \propto U_c^2(\Delta U)^6$, a relation which has also been found in a previously published AWB experiment [4].

An often used diagram type for illustration of the scaling coefficients is the double logarithmic diagram of *OASPL* vs. the *velocity scaling parameter* (see e.g. Harper-Bourne [16, Figs. 10 and 15], Viswanathan [10, Fig. 5], Bridges and Brown [17, Fig. 6]). If enough operations are tested, velocity scaling exponents can be extracted. Take for example the forward arc position, where the exponents 6 for loading noise and 8 for static jet noise are found (see Fig. 4). The rear arc scales with exponents of 8 which is consistent with the fact that in this region the installed jet noise does not differ much from the isolated jet noise.

It can be concluded that there is a systematic difference between forward and rear arc.

B. Scaling coefficients along the flyover arc

The follow up research question is how does the transition of scaling coefficients between forward arc and rear arc look like?

The answer to this question is a diagram of scaling exponents over the full flyover arc. Each exponent is derived from individual OASPL-vs-log(velocity) diagrams at each microphone. With the help of linear regression, velocity scaling coefficients are determined. The two types of comparison are:

1) Find the exponent n in ΔU^n using three test points of the same shear layer convection velocity U_c.
2) Find the exponent m in U_c^m using three test points of the same shear layer difference velocity ΔU.

The exponents m and n, as well as the combined coefficient $(m + n)$ are plotted in Fig. 5 over the measured flyover arc. The main takeaways of this figure are:

1) The n exponents (- - - dashed lines) for *isolated and installed* jet noise are very similar when comparing operations of the same shear layer convection velocities U_c.
2) There is an almost negligible depency on shear layer convection velocity U_c (see the m exponent for the *installed* jet, i.e. the -.-.- gray dash-dot line). This is very relevant for the max. wind tunnel velocity problem in section V.A: It can be concluded that operations with same ΔU produce the same installation noise.
3) The m exponent of *isolated* jet noise ((-.-.- blue dash-dot line) reduces from $m = 2$ in the forward arc to $m = 0$ in the rear arc. Hence, a simple rule like "same ΔU produces the same isolated jet noise" is not generally valid, i.e. only valid in the rear arc.
4) The combination $m + n \approx 8$ for *isolated* jet noise (— blue solid line) agrees with Lighthill's analogy.

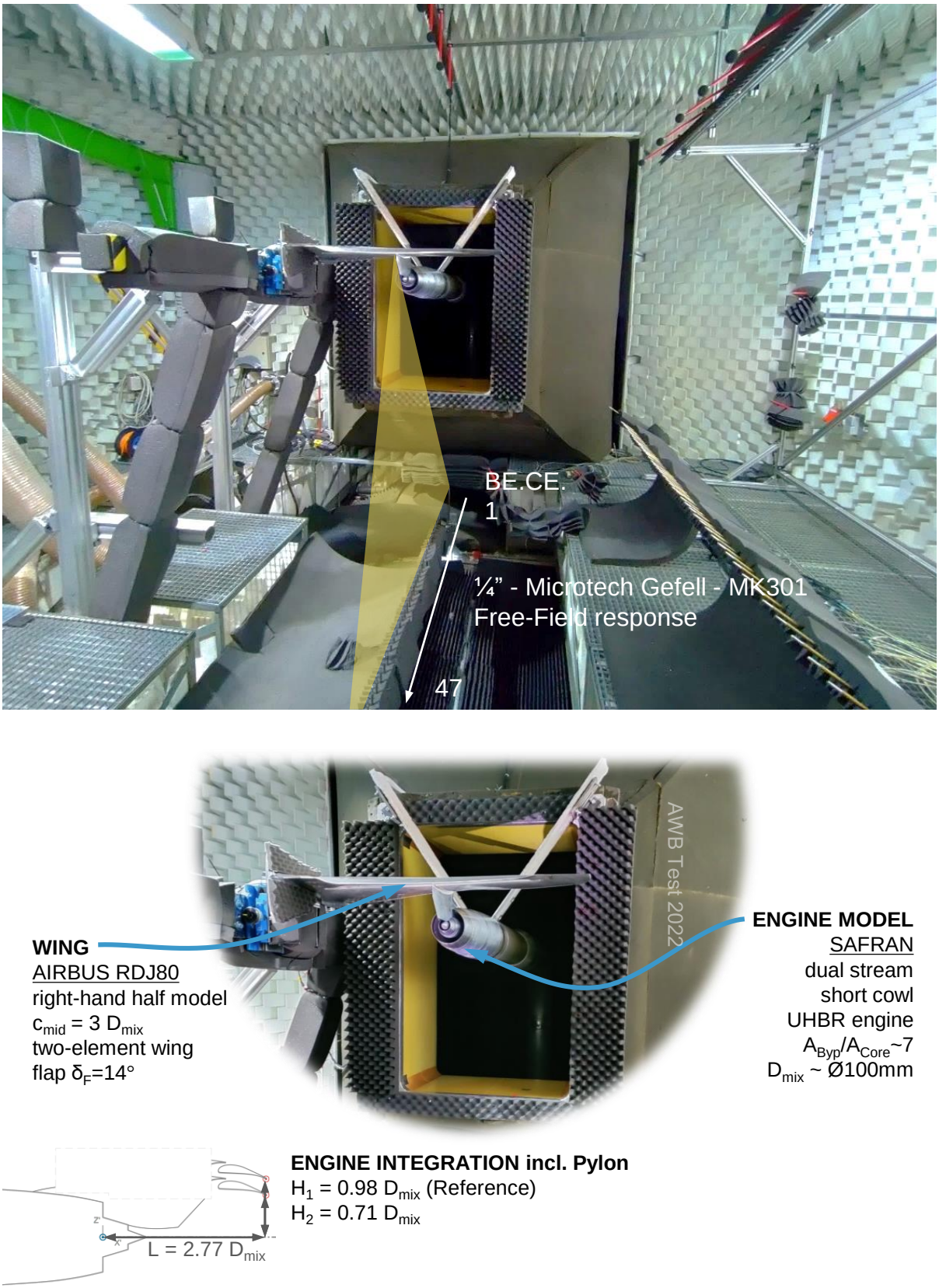

Fig. 3 top image: Instrumented flyover arc in AWB consisting of 47 microphones.
Bottom image: Experimental setup of wind tunnel model. Pictures are AIRBUS DLR and SAFRAN property.

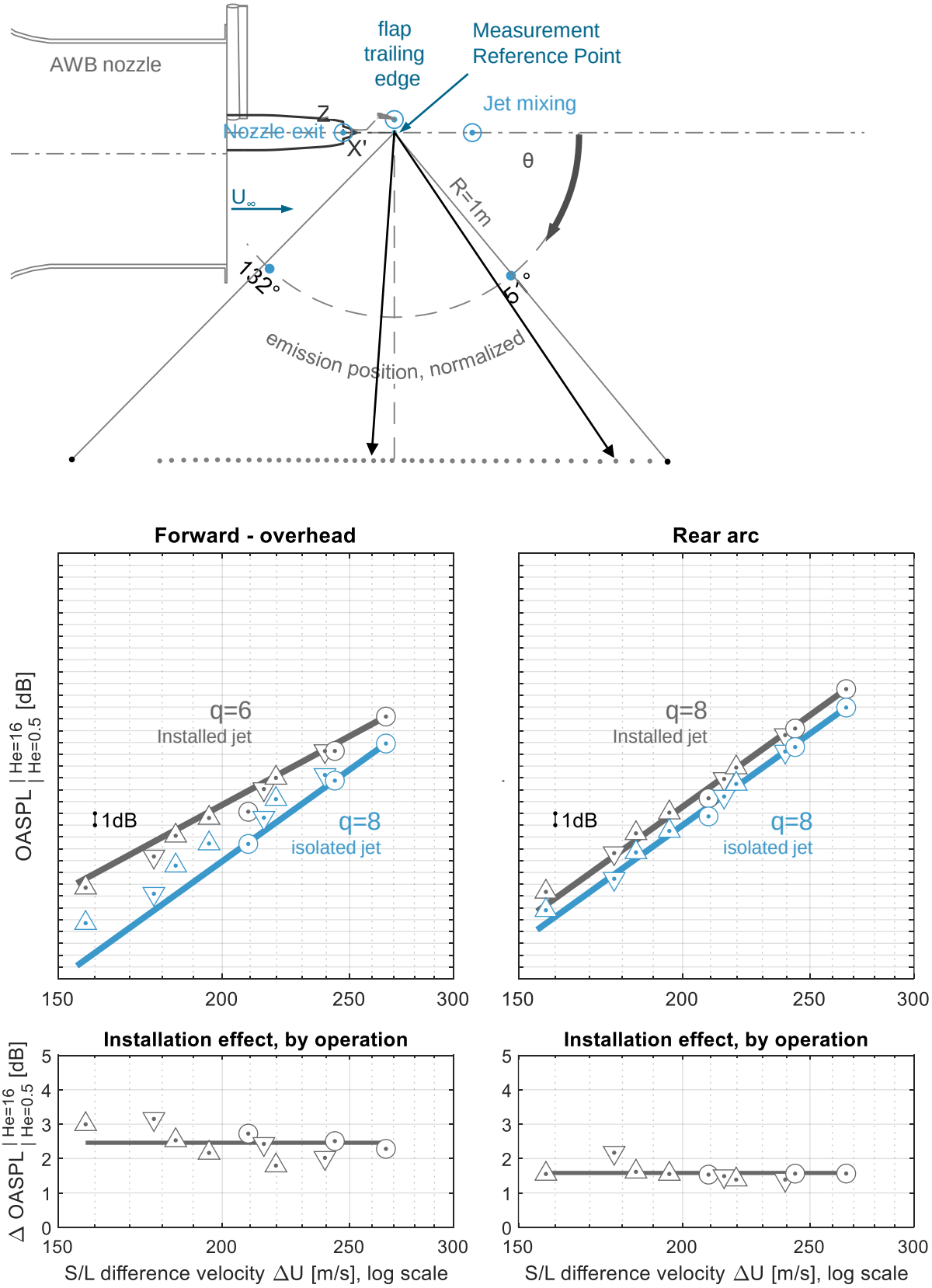

Fig. 4 Velocity scaling for a pylon-integrated engine in the forward arc and rear arc. Markers depend on wind tunnel velocity, as defined in Fig. 2

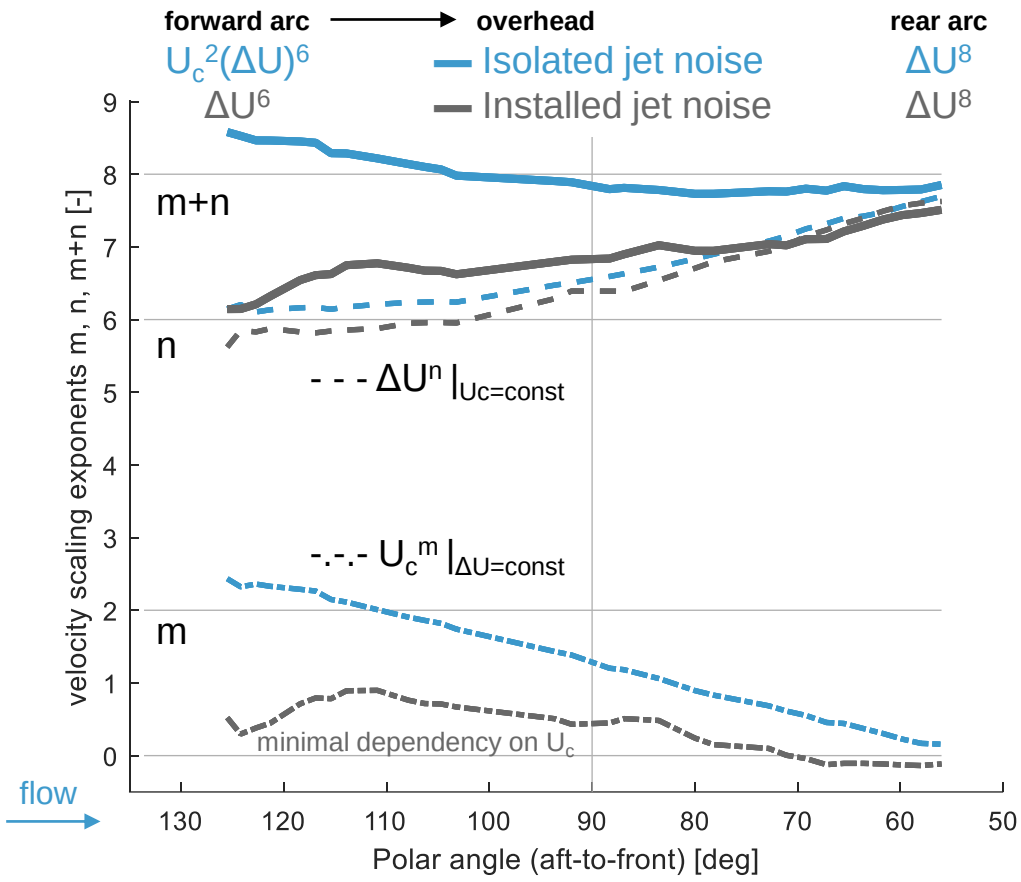

Fig. 5 Velocity scaling for a pylon-integrated engine in the forward arc and rear arc w.r.t. flap trailing edge. Markers depend on wind tunnel velocity, as defined in Fig. 2

.

5) The general trend of a transfer from n=6 (forward) to n=8 (rear) for installed jet noise (— gray solid line) agrees with the trend shown by Brown and Ahuja [18, Figs. 35a and b].

V. Application

The insights from the previous section, i.e. IV, can be used for various fields of application, among others

- to interpolate isolated and installed jet noise data in between the tested operations. A special case of this method is
- to repair spectra with poor signal-to-noise ratio between measured signal and background noise.
- to extrapolate isolated and installed jet noise datapoints to operations which are out of scope for the used test facility. An examplatory case, the max. wind tunnel velocity problem, is presented below.

A. Max. wind tunnel velocity problem

The term "Max. wind tunnel velocity problem" stands here for the research question: How is it possible to cross-compare the test data of the same build from two different test facilities where one facility can test the target wind tunnel velocity of *here* 60 m/s whereas the other one can only reach a smaller wind tunnel velocity, *here* 40 m/s [†]? The reference test operation is defined by a jet velocity of 279 m/s and a wind tunnel velocity of 60 m/s. The evaluation is done at three polar positions, in the forward arc, close to the overhead position and in the rear arc.

Two test points are used to reconstruct the same signal as the reference, one with constant shear layer difference

[†]or, alternatively allows for static operations only

velocity ΔU, and one with constant shear layer convection velocity U_c (see Fig. 6 and Table 1).

1) Test point 1 is defined by the ■ same shear layer difference velocity ΔU and is supposed [‡] to get the gain quantitatively right. Overall sound pressure levels agree with the reference testpoints at an accuracy of 0.3 dB. The spectral shape functions collapse well within ±1 dB in the rearward arc, where $I \propto (\Delta U)^8$ is expected. The forward arc collapse of ±2 dB is ok for the low-frequency loading noise part $I \propto (\Delta U)^6$. However, the forward arc high-frequency signal is too low by 2 dB. Assuming a jet-noise like analogy $I \propto (\Delta U)^6 U_c^2$, the higher wind tunnel setting produces more noise than the lower wind tunnel setting.
2) The prediction can be improved, when starting with test point 2, a high thrust data point. It features the ■ same shear layer convection velocity U_c and generates spectral shape function which are similar to the reference. The shape functions of test point 1 must be significantly corrected by $n \cdot 10 \cdot \lg(\Delta U)$. This is difficult, since knowledge about the velocity scaling coefficient $n = 6 \ldots 8$ for ΔU is necessary. In this example, it means to subtract 4 dB (n=6) to 5.2 dB (n=8) from the test point 2 signal in order to approximate the reference signal. Here, we just "trust literature" (option A) and use the ΔU^n-exponents for const. U_c derived in Fig. 5 and listed in Tab. 1, line 2. Overall sound pressure levels do also agree within a range of 0.3 dB - this is the same value as for the other method. An improvement is the collapse of third-octave spectra which is good within ±1 dB in the forward and rear position. The shape functions are mainly preserved. The greatest shape error is caused in the forward arc high-frequency region.

All in all, the cross-comparison with test point 2 improves the third-octave band spectrum accuracy for predicting the max. wind tunnel velocity problem. However, alternatives to option (A) could be considered:

- Option (B) is to measure test point 1 in addition to test point 2. This helps to get direct experimental information about the expected OASPL. There is no need to refer to ΔU-velocity scaling coefficients from other sources. This is especially helpful, if there are large ΔU-corrections, e.g. for the extrapolation from static to flight conditions.
- Simply assuming the mean velocity scaling coefficient of n=7 for the entire arc (Option C) will *here* produce errors of +0.6dB (forward) and -0.6dB (rear) between prediction and reference.

Table 1 Max wind tunnel problem analysis, deviations to reference (■ gray)

Position	**forward**	**overhead**	**rear**
polar angle, emission (aft-front)	126°	96°	57°
ΔU-Velocity scaling exponent	6.2	6.5	7.7
Test point 1 (■ yellow): ΔU ≈const			
ΔU-Correction	0.5 dB	0.6 dB	0.7 dB
Spectral collapse third-octave	-1.8 . . . 2.1 dB	-0.9 . . . 2.0 dB	-0.8 . . . 1.2 dB
ΔOASPL w.r.t. Ref.	0.2 dB	0.1 dB	0.3 dB
Test point 2 (■ green): U_c ≈const.			
ΔU-Correction	−4.1 dB	−4.3 dB	−5.1 dB
Spectral collapse third-octave	-1.1 . . . 1.2 dB	-0.5 . . . 0.5 dB	-0.8 . . . 0.2 dB
ΔOASPL w.r.t. Ref.	−0.1 dB	0.0 dB	−0.3 dB

[‡]In this particular test case, there is a slight offset in ΔU, which is why the slight gain correction of 0.6-0.8dB is included.

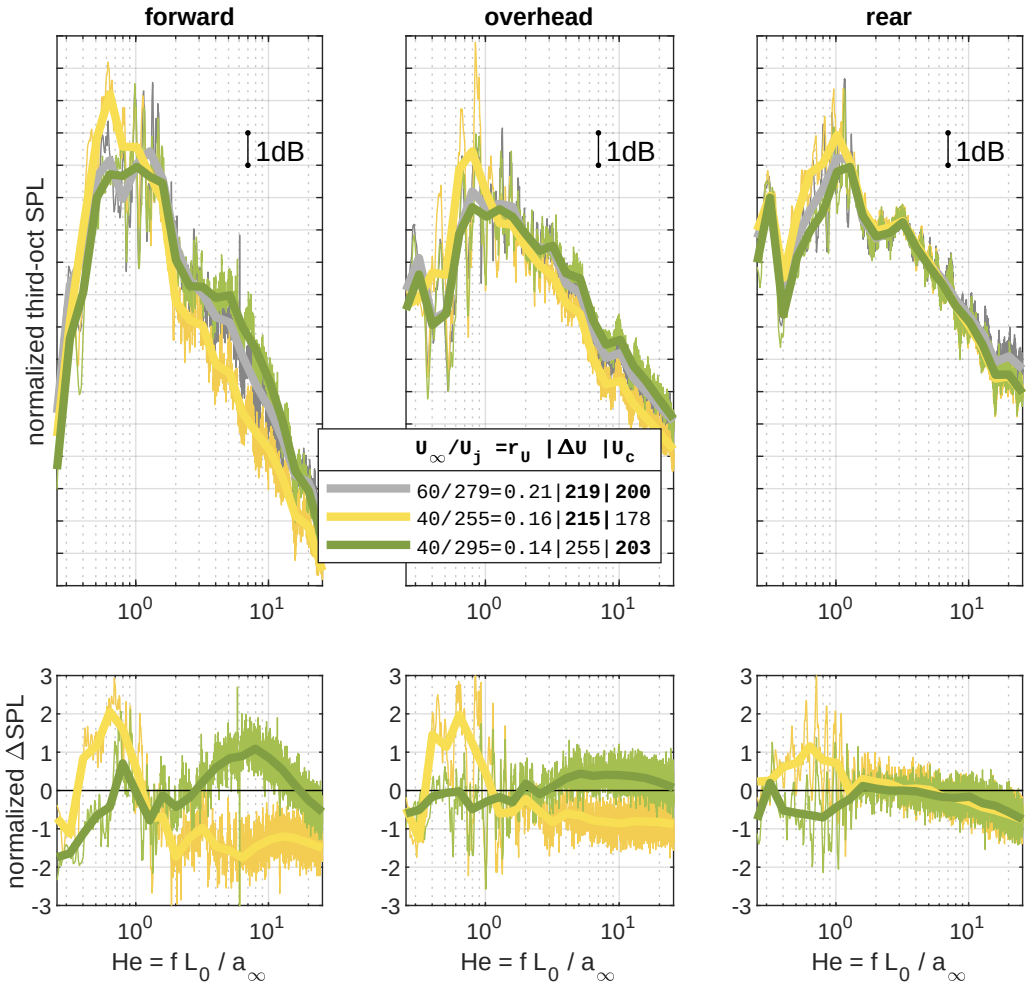

Fig. 6 Max wind tunnel velocity problem. gray: ■ reference test at high wind tunnel velocity, yellow: Conventional replication with a lower wind tunnel velocity using the ■ same shear layer difference velocity, green: Improved prediction using the ■ same shear layer convection velocity. Top row: shape functions for three different polar angles. Bottom row: Deviation of predictions from reference.

VI. Discussion of applicability limits

There is a great temptation to transfer a successful method to related physical problems. This must be done with great care, since there are limits in the applicability. The presented source mechanisms, a combination of loading noise and jet noise like terms in the flyover arc, model the installed jet noise of the pylon-integrated engine on a two-element wing (with main wing and flap). Some seemingly related installation problems may depend on other significant noise sources:

- Sengupta [1, Fig. 14] listed two types of noise mechanisms which could either dominate the high-frequency part of the spectrum: **reflected jet noise** as well as **trailing edge noise** (or generally speaking installation noise). A realistic wing contains various trailing edges which need to be checked for relevant contribution to the installation noise. Side edge noise may be caused by a small gap or wide gap (thrustgate configuration) between flap 1 and flap 2. A closeby installed flap track could also increase the engine installation noise.
- The AWB experiments with three-element wings (slat - main wing - flap) captures high-lift wing noise which is mainly related to the slat. The slat plays a crucial role for high velocity ratios. Jente [19, pp. 42-46] described a method on how to determine the insignificance limit of the high-lift wing related noise.
- More "academic" installations where engine and wing are unconnected/freely positioned to each other, i.e. without pylon, produce significantly greater tonal and broadband excess noise. This effect has been published by many authors, e.g. EU-project Jeronimo CEPRA-19 test data by Davy et al. [20, Fig. 15], Lawrence [21, pp. 153-157] or even distinction between weak and strong tones Amaral et al. [22, Fig. 12]. Other available data stems from the DJINN-JExTRA experiment [23]. Qualitative differences between engine integrations that use or lack a pylon are studied in more detail in the section below.

A. Acoustic effects without the pylon

The velocity scaling is done with the purpose of allowing a qualitative[§] evaluation of the pylon installation effect by comparison with section IV.A. The JExTRA experiment is limited to static operations only. The polar angles for the forward and rear arc positions were chosen to be roughly comparable. Installed jet noise data is evaluated with and without tone removal (method is described in [23, pp. 11-12]).

The installation and the velocity scaling are shown in Fig. 7 and allow the following conclusions:

1) The forward arc velocity scaling coefficient equals 6 for both, the pylon-integrated installation and the non-tonal JExTRA installation data. The tones change the velocity scaling coefficient towards 8.
2) The rear arc installation effect for both experiments does not differ much from jet noise and follows approximately the exponent of n=8.
3) The forward arc installation effect without pylon of 10-15 dB is much larger comparedto the 2-3 dB of the pylon-integrated test. What is the reason for this discrepancy?

This question is attempted to be answered with the steady flow analysis.

B. Steady aerodynamics

Steady aerodynamics data was measured with a DLR total pressure rake. The results are presented in Fig. 8 using velocity contours selective to critical jet velocities. Three of the characteristical geometric build properties (see Eq. 1) are affected by the pylon installation:

1) The mixed jet radius near pylon is smaller since the pylon blocks a portion of the bypass nozzle exit area, creating a jet which is not round (aspect ratio between with to height of 1.1). The blockage contributes to the characteristic rooster-tail effect [25] [26].
2) There is a bypass jet deflection effect of approximately 1°. The jet is deflected away from the pylon of the isolated engine. The downstream deflection has been reported by Faranosov et al. [24, Fig. 6 (ii)] who also showed for the installed jet that this deflection is either neutralized or may even change towards the wing.
3) The near field virtual S/L origin (see Fig. 1) between bypass and flight stream is not constant along different azimuthal positions. Since the pylon blocks the engine exit, the near field S/L on the pylon side (Z^+) cannot develop close to the engine exit - contrary to the side opposite of the pylon (Z^-). This causes asymmetry in the near field shear layer[¶].

Another engine operations related property might affect the installation noise: How does the engine flow deal with the wake behind the pylon? Is it claimed by the bypass stream or by the core stream? The aerodynamic results show

[§] An even better designed experiment for direct quantitative comparison of the pylon effect was conducted by Faranosov et al. [24].

[¶] Other cases of asymmetry at the nozzle lip are the beveled nozzle or part chevrons.

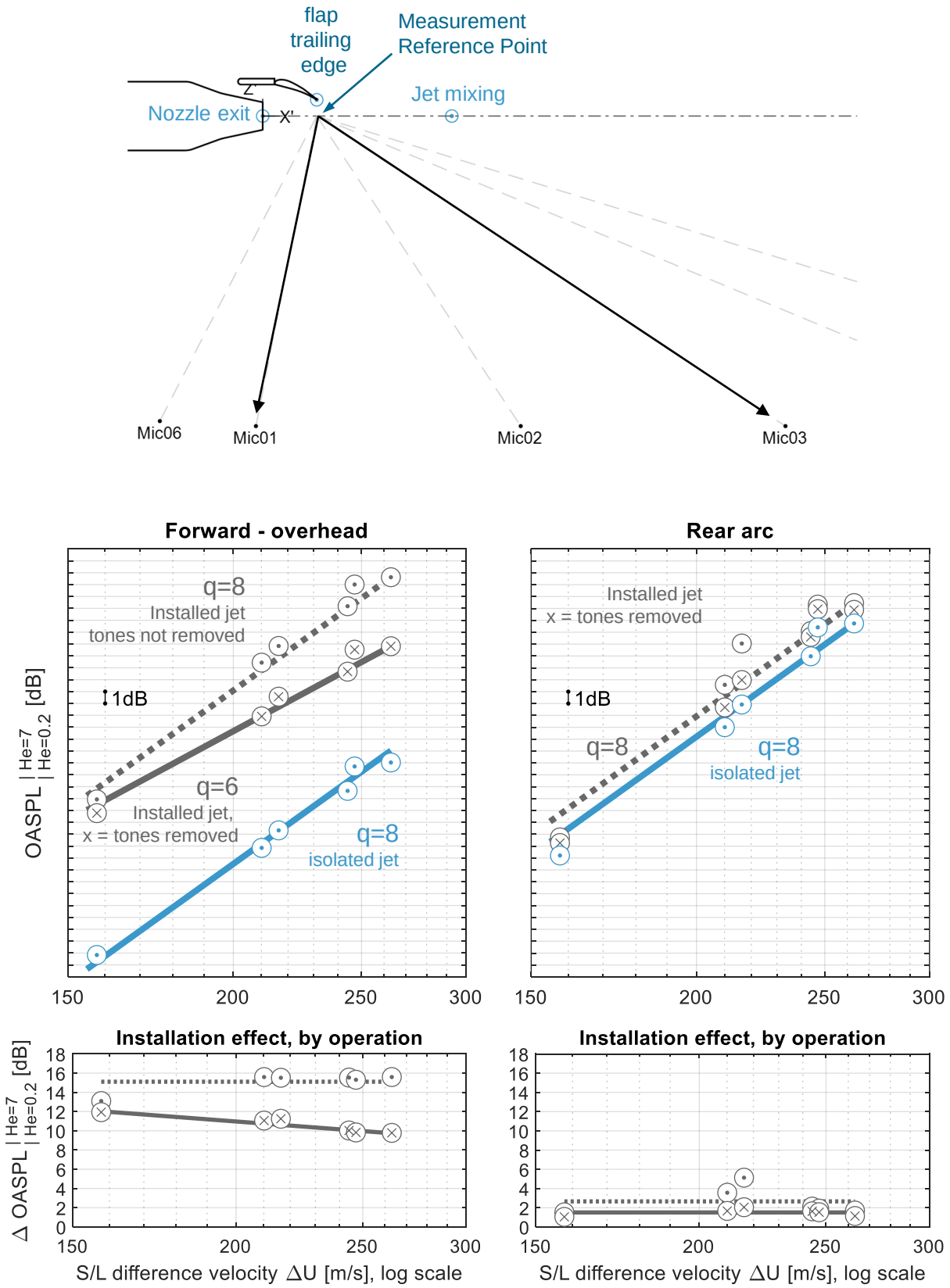

Fig. 7 Velocity scaling for an engine integration without pylon in the forward arc and rear arc. Outer markers indicate static operations only, inner markers the option of using a tone removal tool.

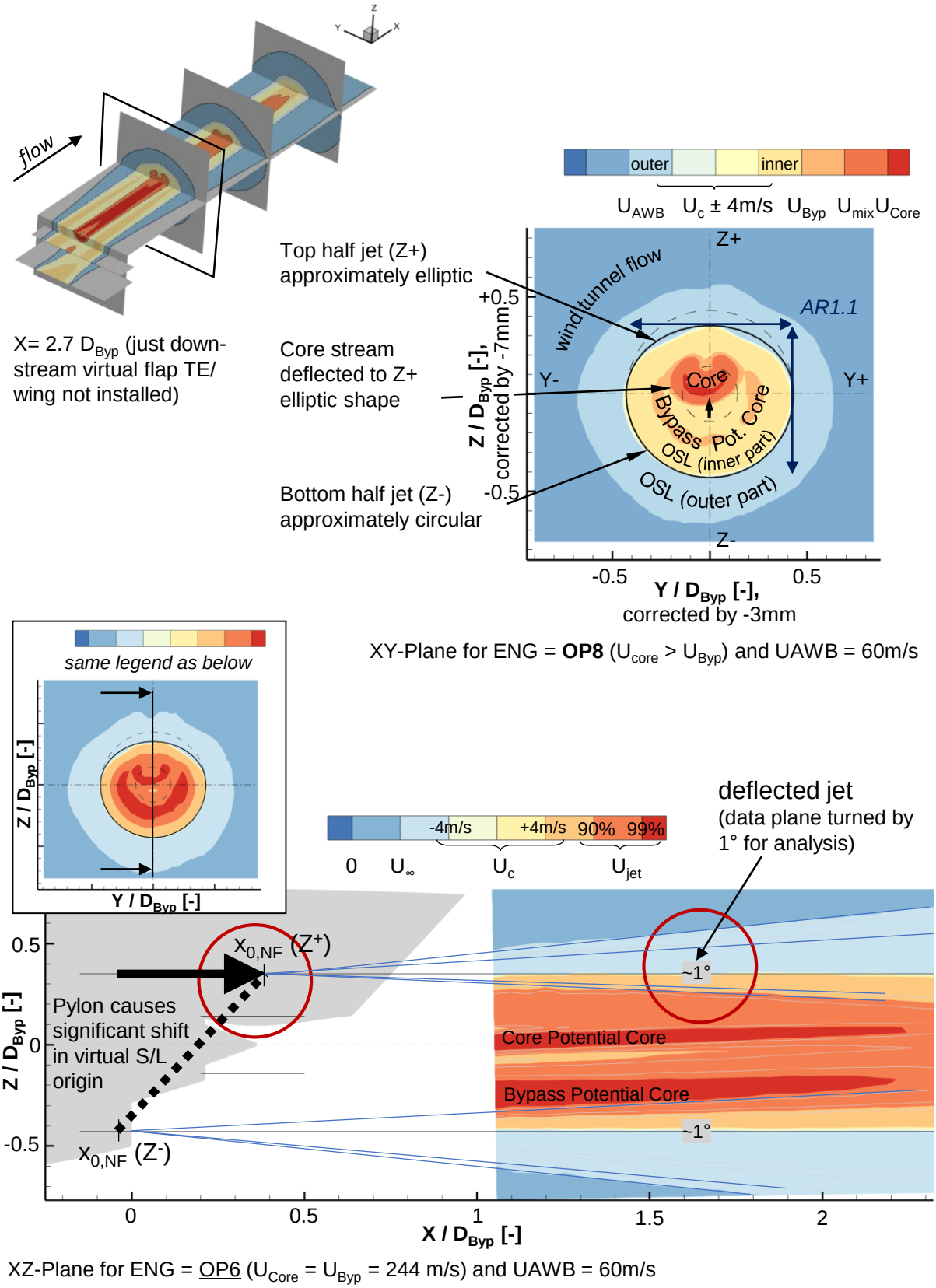

Fig. 8 Steady aerodynamics results for an isolated engine with pylon. Analysis of characteristical velocities of a jet in planes normal to the jet (top) as well as in streamwise direction (bottom) for a same speed jet.

that the core stream is curved (bell-shape): It deflects from the engine axis towards the flap (see Fig. 8, mid), yet further downstream, the flapward movement is reversed. The core stream of a pylon-mounted dual stream nozzle might influence the jet installation noise, potentially posing a problem for the transfer of cold to hot jet noise experiments. Cold dual stream engine models without any pylon can argue with preservation of local similarity (as shown in [27] based on the concept of George [28]). However, a deeper analysis of the core stream effect on installation noise is out of scope for this paper. The data analysis in this paper is conducted with same speed jets (SSJ) only, i.e. where bypass velocity equals core velocity.

C. Aero-geometric characterization of the pylon integrated engine

The conventional aero-geometric characterization (Eq. 1, see also [19, Fig. 3.7]) used for the freely positioned engine integration delivers comparable acoustic installation angles ϕ' between the JExTRA (3°) and AWB experiment (4°). This falsely indicates a certain acoustic comparability.

$$\tan(\phi') = \frac{H - R_{mix}}{L - x_{0,NF}} \tag{1}$$

Hence, a great improvement for a model prediction is the adapted calculation of the installation angle for the pylon-integrated engine (Eq. 2):

$$\tan(\phi') = \frac{H - R_{mix}(Z^+)}{L - x_{0,NF}(Z^+)} \tag{2}$$

- The mixed jet diameter close to the flap $R_{mix}(Z^+)$ can be roughly approximated from CAD: engine exit areas need to be constructed and measured (including and excluding the blockage of the pylon). The discharge jet is assumed as a semi-elliptical, semi-circular discharged jet as in Fig. 8, mid.
- Slight shifts of the virtual shear layer origin from the engine lip can often be neglected. Yet, the blockage of the pylon causes a larger shift from the bypass engine lip (Fig. 8, bottom) towards the midst of the pylon. This property can only be very roughly approximated near the x-position of the core nozzle.

VII. Conclusion

This paper contributes to the ongoing research with an analytical derived analogy for the far-field noise of installed jets. The pylon-integrated engine installations either do not differ much from jet noise (exponent 8 in the rear arc) or transition towards the exponent for loading noise (exponent 6 in forward-to-overhead position).

Operations with same near field shear layer convection velocity U_c provide master shape functions for each polar angle. This benefits the the prediction of absolute JFI noise gains, especially in the forward to overhead arc. A potential takeaway is to include U_c as a test parameter in future test campaigns.

Scaling exponents were determined over the entire flyover arc. Fig. 5 is presumably the first published visual representation of the shifting velocity scaling laws for both isolated and installed jet noise at flight operations. The combination of improved velocity scaling approach together with the analytical derivations is a suitable tool in the search for underlying physics.

The results benefit the empirical prediction methods: In an examplatory case of the max wind tunnel problem, an improvement in prediction uncertainty of an extrapolated installed jet noise datapoint was demonstrated.

The applicability limits of the derived analogy w.r.t. related problems was shown, especially the effect of a pylon and non-pylon integrated problem: The pylon effect simplifies the acoustic characterization, but complicates the aero-geometric characterization.

The presence of the pylon is the reason for asymmetric jet properties which especially affect the spatial region close to the flap. Hence, a significant reduction of the feedback mechanism causes *here* only a remarkably unimpressive mid-frequency installation effect. The asymmetries were included as part of an improved aero-geometric characterization of the installation angle.

An unreviewed issue is the role of the core jet towards installation noise. Since the flow analysis indicates a turn in flap direction just downstream the pylon, the hypothesis is that the core velocity may significantly influence installation noise. "What is the influence of the core stream w.r.t. the installation noise of pylon-integrated engines?" is therefore an interesting candidate for follow-up research.

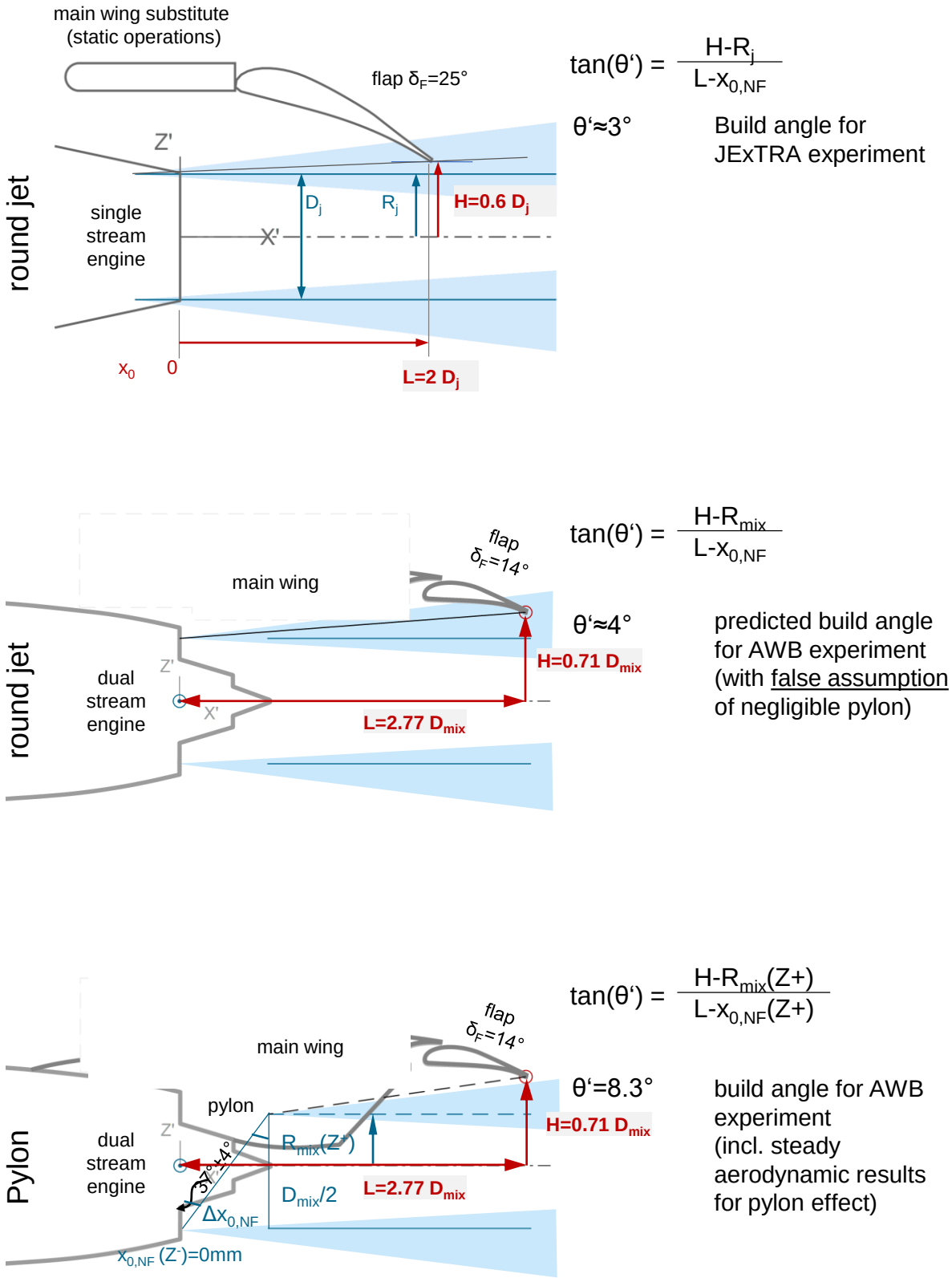

Fig. 9 Aero-geometric characterization of JExTRA experiment (top) and transfer to the AWB experiment without the pylon effect (mid) as well as including the aerodynamic results from Fig. 8 (bottom).

Appendix A: Analysing jet installation noise for compactness

For reason of consistancy, this section uses the notation and partial wording of a university lecture script Delfs [29, p. 126] for velocity scaling of loading noise in general. Yet, the approximations are adapted for the jet installation effect discussed in this paper.

Fixed and rigid objects such as the wing and its flap generate excess noise due to the interaction of the body surface with unsteady flow fluctuations. The far-field solution has been derived by Curle and Lighthill [30] as well as Ffowcs Williams et al. [31] (see Eq. 3).

$$p' \simeq \underbrace{\frac{1}{4\pi a_\infty^2 r_0}(\boldsymbol{e}_{r_0}\boldsymbol{e}_{r_0}) : \frac{\partial^2}{\partial t^2}\int_{V'_\infty} \boldsymbol{T}\, dV}_{\text{(1) free turbulence}} + \underbrace{\frac{1}{4\pi a_\infty r_0}\boldsymbol{e}_{r_0} \cdot \frac{\partial}{\partial t}\int_{\partial V_B} (p\boldsymbol{I} - \boldsymbol{\tau}) \cdot \boldsymbol{n}\, dS}_{\text{(2) excess noise due to presence of object B}}. \tag{3}$$

Term (1) represents Lighthill's [32] solution for noise generated aerodynamically, which leads to the well-known result of free turbulence scaling with the eighth power of the characteristic velocity. This term is very significant for the rear arc as well as the high frequency region of the forward arc.

Term (2) is relevant for installation noise in the forward arc. It describes additional noise which is induced by the presence of the object. Especially the low-frequency part of the spectrum is of interest: the surface as a noise source is called *compact* for frequencies lower than the characteristic frequency.

The characteristic distance is roughly the engine integration length L. [‖] The characterizing frequency f_c is calculated with $He = 1$ to $f_c = a_\infty / L$.

The integral in term (LF) is interpreted as the net aero force on the body $\boldsymbol{F}$. The vector $\boldsymbol{e}_{r_0}$ accounts only for the net aero force component in the direction of the observer, therefore labeled as F_{r0}.

$$p'_{(2)} \simeq \frac{1}{4\pi a_\infty r_0}\frac{dF_{r0}}{dt} \tag{4}$$

The sound field is directly proportional to the time change of the net aero force on the body. w.r.t. jet-flap interaction, Sengupta [1] detected the same mechanism and called it lift fluctuation noise.

The magnitude of the aerodynamic force is estimated by the following jet parameters acting on a partial flap surface:

$$|\boldsymbol{F}| \propto \rho_{flap} U_{flap}^2 S_{flap} \tag{5}$$

Each parameter with index *flap* serves as a placeholder which should be proportional to some test parameter:

- We assume that the velocity fluctuations can be approximated by the shear velocity ΔU. Alternatives are challenged with experimental data in section II.
- The interaction area is *here* very roughly approximated as half perimeter of the jet ("along flap span") and shear layer width ("along flap chord") δ_ω. The shear layer width (and hence the relevant interaction area) changes w.r.t. velocity according to thin mixing layer theory (e.g. Eisfeld [34] by $\delta_\omega \propto L_0 \Delta U / U_c$

  $$S_{flap} \propto \pi R_{mix} \delta_\omega \propto \pi R_{mix} L_0 \Delta U / U_c \tag{6}$$

  This approximation is sufficient for the purpose of this paper, but should be expanded to include build sensitivities, such as engine integration height.
- In order to account for differences in static temperature between jet stream and flight stream, the density term is approximated as a mix between the two streams:

  $$\rho_{flap} = \sqrt{\rho_j \rho_\infty} \tag{7}$$

  Since the AWB test delivered only cold test data, the relation cannot be well proven or disproven. Hence, this term does not get further attention within the paper.

[‖] For detailed types of analyis, it can be benefitial (Jente et al. [23, p. 15]) to substitute L with $L_0 = L - x_{0,NF}$, where $x_{0,NF}$ is the virtual shear layer origin of the outer shear layer $x_{0,NF}$. The virtual shear layer origin can be determined by analysing the steady aerodynamic flow downstream the engine (Jente [33]) and its X-position is here located roughly at the midst of the pylon.

All in all, the magnitude of the force is estimated as

$$|\boldsymbol{F}| \propto \sqrt{\rho_j \rho_\infty} \frac{(\Delta U)^3}{U_c} \pi R_{mix} L_0 \tag{8}$$

The time change of the force occurs during the characteristic period t_c it takes to convect a flow disturbance along the wing**, i.e. $t_c \propto L_0/U_c$. There is a link between the two indeed : if we study wing lift fluctuation noise, the hydrodynamic wavelength is assumed to be greater than the wing chord. This relation is used to approximate the time derivative $\frac{\partial}{\partial t} \propto 1/t_c = U_c/L_0$.

The sound intensity of a compact body scales like

$$I = \overline{p' v'_{r0}} \simeq \frac{\overline{p'^2}}{\rho_\infty a_\infty} \tag{9}$$

$$\boxed{I \propto \frac{{R_{mix}}^2}{r_0^2} \frac{\rho_j}{a_\infty^3} (\Delta U)^6} \tag{10}$$

The sound intensity of the compact installation noise for scales with the sixth power of the difference velocity ΔU.

For purpose of analysis, it can be beneficial to decompose sound intensity into the following factors: Flight operations effect $\mathcal{F}$, Temperature effect $\mathcal{T}$ and Geometry $\mathcal{G}$. This is done by using the relations $\rho_j = \gamma_j p_\infty / a_j^2$ (i.e. ideal gas and definition of speed of sound) as well as $\Delta U = U_j(1 - r_U)$ with the velocity ratio between the flight velocity and the jet velocity $r_U = U_\infty / U_j$:

$$I \propto p_\infty \frac{{R_{mix}}^2}{r_0^2} \frac{\gamma_j}{a_j^2 a_\infty^3} U_j^6 (1 - r_U)^6 \tag{11}$$

Furthermore, the aerodynamic jet Mach number $M_j = U_j/a_j$ as well as the acoustic Mach number $M_{ac} = U_j/a_\infty$ are introduced (same procedure as by Jente [36]).

$$I \propto p_\infty U_j \underbrace{\gamma_j M_j^2 M_{ac}^3}_{\mathcal{T}} \underbrace{(1 - r_U)^6}_{\mathcal{F}} \underbrace{\frac{{R_{mix}}^2}{r_0^2}}_{\mathcal{G}} \tag{12}$$

**This is a rather conservative approximation: More precisely, the origin for lift changes over time relates to the hydrodynamic wavelength, which is assumed to be even greater than the wing chord, e.g. by factor 2 for a Mach 0.6 subsonic jet [35].

Appendix B: Velocity scaling of forward arc jet installation noise - experimental proof

Finding the velocity scaling of JFI noise is an iterative process which consists of formulating a test hypothesis (here based on the analytical derivation in section VII) and challenging the hypothesis against experimental data.

The initial derivation process in section VII produced the following velocity candidates:

- shear layer difference velocity $\Delta U = U_j(1 - r_U)$
- shear layer convection velocity $U_c = U_j(r_U + \alpha(1 - r_U))$, with $\alpha = 0.64$ [††].
- operations which produce approximately the same thrust can be detected by calculating $U_{th} := U_j\sqrt{1 - r_U}$

In order to force a smart observer position, one velocity candidate is kept constant at a time while other velocity candidates and scaling exponents are varied. The uncertainty and quality of the found scaling exponent depends on the gain difference ΔSPL_0 of the unscaled data.

1) The process starts with finding the combined velocity scaling exponent by cross-comparing the **same velocity ratio operations**, i.e. r_U = const. Since these velocity profiles are self-similar, it does not matter which velocity candidate is used for scaling, all parameters have the same proportionality to each other. This includes the set of the tested quasi-static conditions ($r_U \approx 0.04$, see Fig. 10): The low-frequency noise $He < 1$ scales with a velocity exponent close to $q = 6$. The high-frequency spectrum scales with exponent $q = 8$, which is the expected result for free turbulence (term (1) in Eq. 3).
2) Then, operations with **constant shear layer convection velocity** are chosen.
   Note, that the relevant surface area depends on velocity components (Eq. 6). If this surface area was assumed invariant to velocities instead, the sound intensity would be proportional to $U_c^2(\Delta U)^4$. This is why $q = 4$ is checked, as well as $q = 5$ (trailing edge noise) and $q = 6$ (compact noise, as derived in Eq. 10).
   The scaling for $U_c = 180\,\mathrm{m/s}$ (see Fig. 12) collapses well for $(\Delta U)^6$. Note, that this does not only affect low-frequency noise, but the entire spectrum. This is no accident, since jet shear layer noise has been reported to scale as $I \propto U_c^2(\Delta U)^6$. (see Jente and Delfs [4] for low r_U or Michalke and Michel [15, Eq. 4.31 for $A \approx 1.6$)].
   Note, how similar the shape functions are. One might come up with the idea to identify shape functions for all U_c and use them for modelling the JFI effect. However, it must be admitted, that the operations are not too different (scaling difference is only 3dB, not 10dB). Hence, more than one U_c has to be checked for its shape.
3) The ultimate prove for dependence on ΔU alone is testing operations with **same shear layer difference velocity**. According to Eq. 10, these profiles should collapse by default and show a gain difference close to zero. It cannot be denied that the shape functions do not match well and that there is a slight dependency on U_c (see Fig. 5, -.-.- gray dash-dot line).
4) In order to remove any doubt on the approximation of the relevant flap velocity, checks can be made to rule out the thrust option $|\boldsymbol{F}| \propto U_j\Delta U$, e.g. by using **same jet velocity** operations. There is another advantage of this test compared to 2.: The gain difference of the data to be scaled is very large. Hence, there is greater certainty in the determined scaling exponent.
   The exponent $q = 4$ supports a dependency on jet thrust, $q = 6$ loading noise and $q = 5$ trailing edge noise.
   According to the results in Fig. 14 for $q = 4$, the dependency on thrust can be ruled out. Moreover, $q = 5 \ldots 6$ scales very nicely for the high frequencies, since the conditions are jet-noise like (compare Michalke and Michel [15, Eq. 4.31 for $A = 1$]). However, the shape functions for $He < 1$ vary and look a bit better for same shear layer convection velocity (Fig. 12).
5) With the same reason as in 4., operations with **same wind tunnel velocity** U_∞ can be checked. There is also the advantage of large gain difference (8 − 9 dB). Note, that Brown and Ahuja [18, Fig. 34] found a power 6 dependency on jet velocity U_j for U_∞ =const.
   The low-frequency scaling looks promising for both $q = 5$ and $q = 6$ (see Fig. 15). The case of same wind tunnel velocity was also studied by Brown and Ahuja [18, Fig. 34]. They found a power 6 dependency on jet velocity U_j for peak noise. This dependency does not contradict the dependency on ΔU, since the scaling coefficients for U_j and ΔU do not differ much for this special case: $U_j^6|_{U_\infty=40\,\mathrm{m/s}} = \Delta U^{6.4\ldots6.2}$ for jet velocities in the range of $U_j = 150 \ldots 300\,\mathrm{m/s}$.

The following figures 10 to 15 show third-octave sound pressure level as gain. The $\Delta f = 10\,\mathrm{Hz}$ narrowband data is shifted (see Gaeta and Ahuja [38]) in order to match the shape of the third octave spectrum. The right diagram features the scaling of two or three promising velocity exponents q.

[††]This value is very close to Fuchs and Michel [37, $\alpha = 0.65$, p. 1]

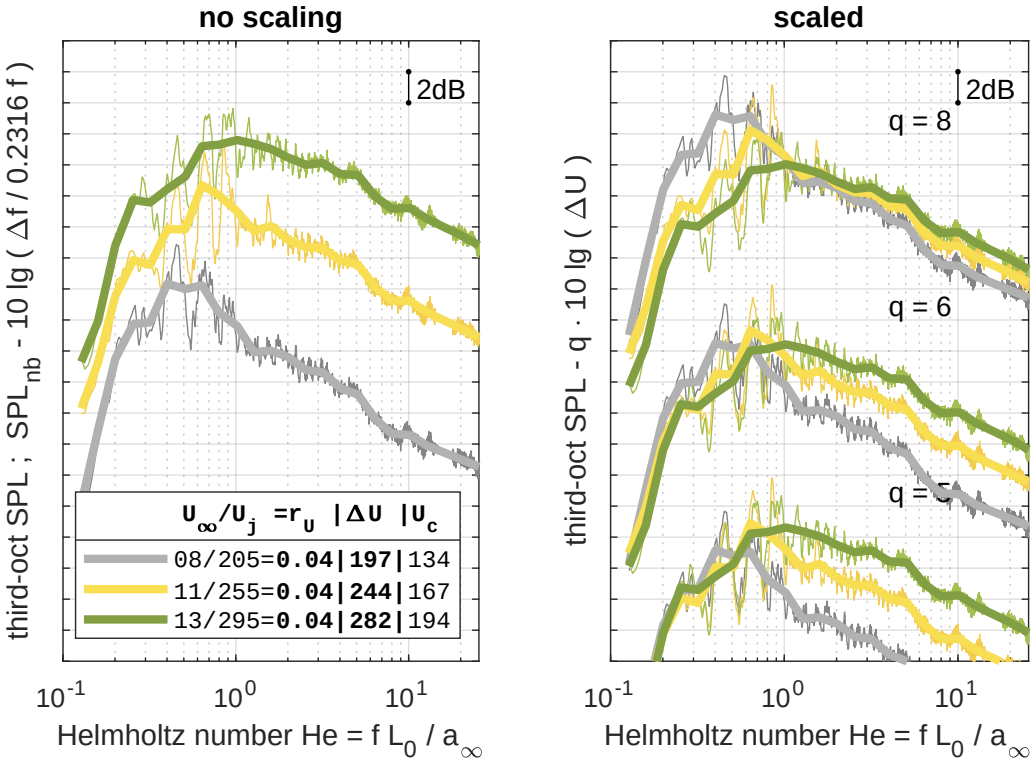

Fig. 10 Same velocity ratio $r_U = 0.04$ (wind tunnel off)

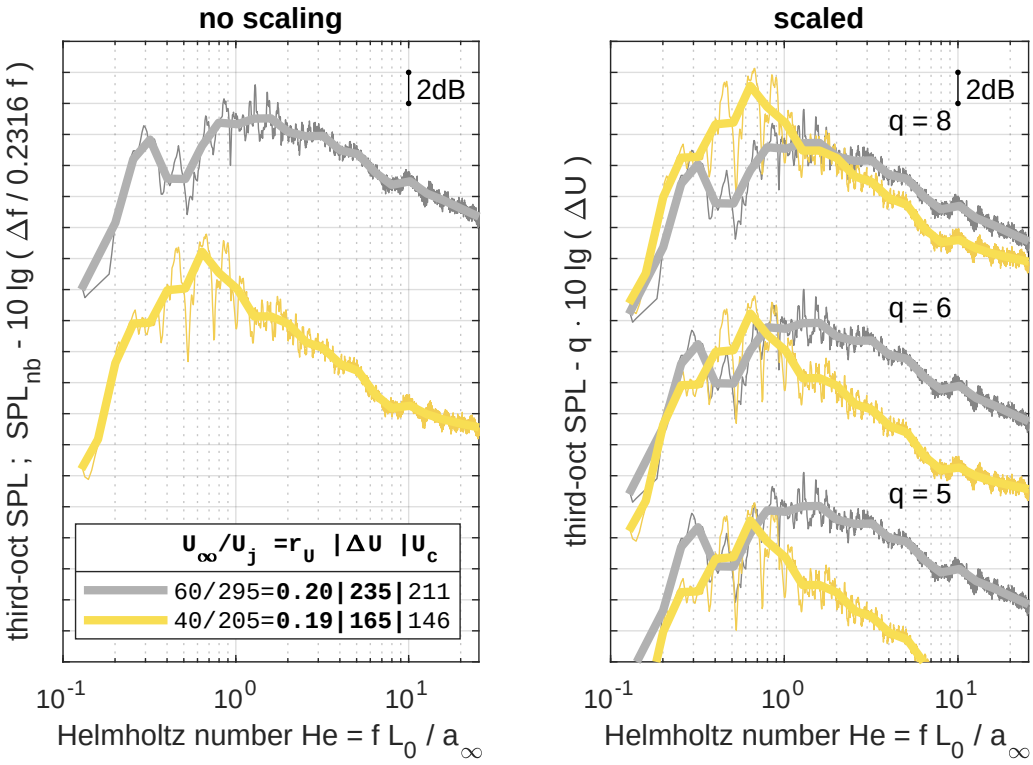

Fig. 11 Same velocity ratio $r_U = 0.20$

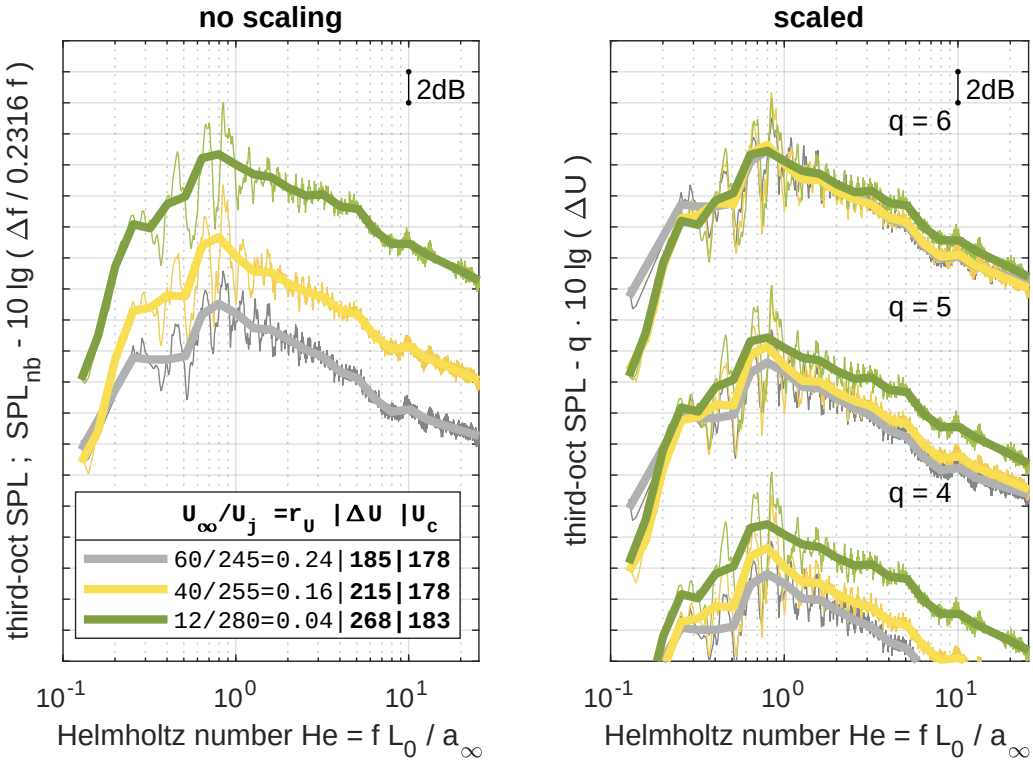

Fig. 12 **Same shear layer convection velocity** $U_c \approx 180\,\mathrm{m/s}$

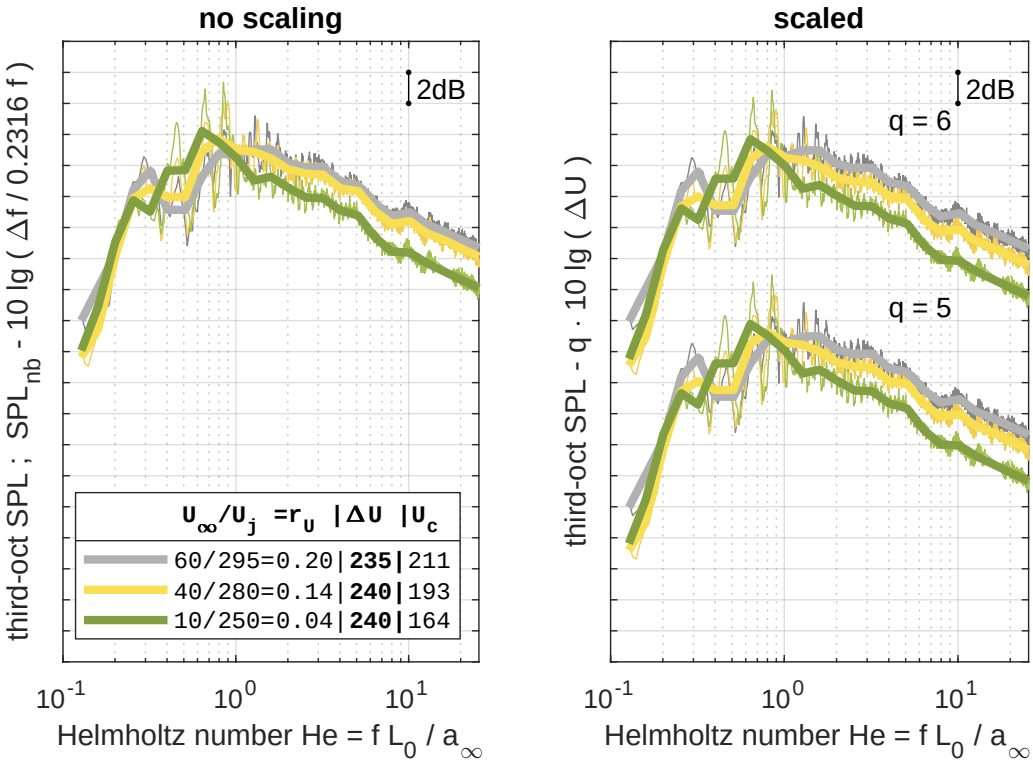

Fig. 13 **Same shear layer difference velocity** $\Delta U \approx 240\,\mathrm{m/s}$

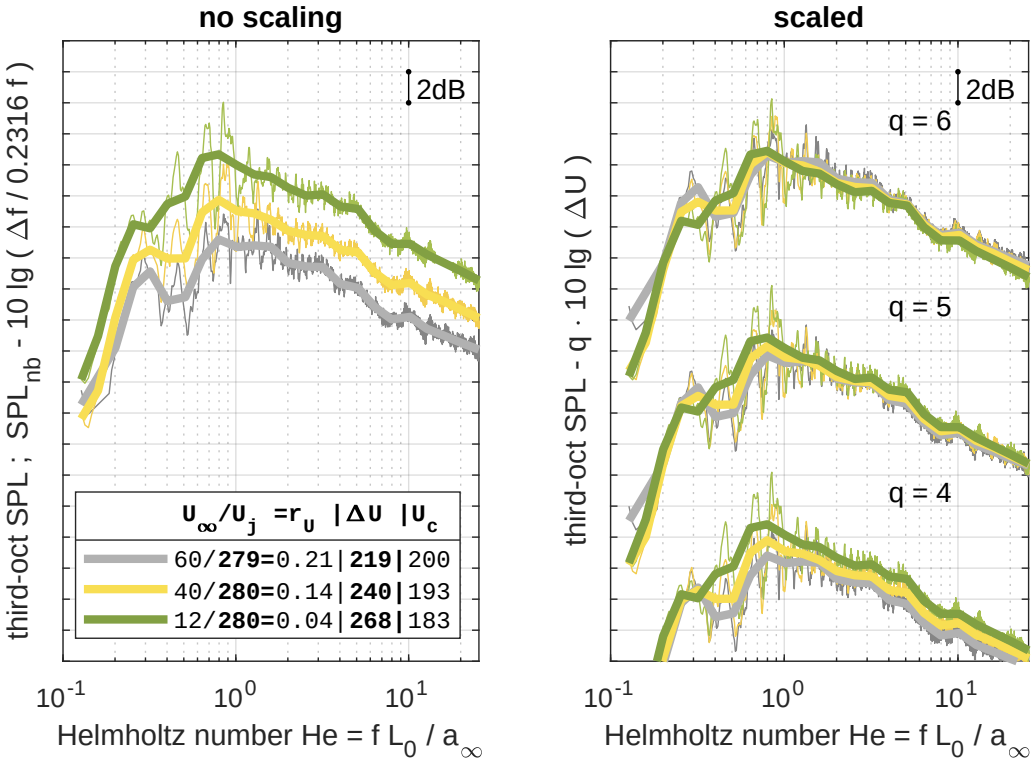

Fig. 14 **Same jet velocity** $U_j \approx 280\,\mathrm{m/s}$

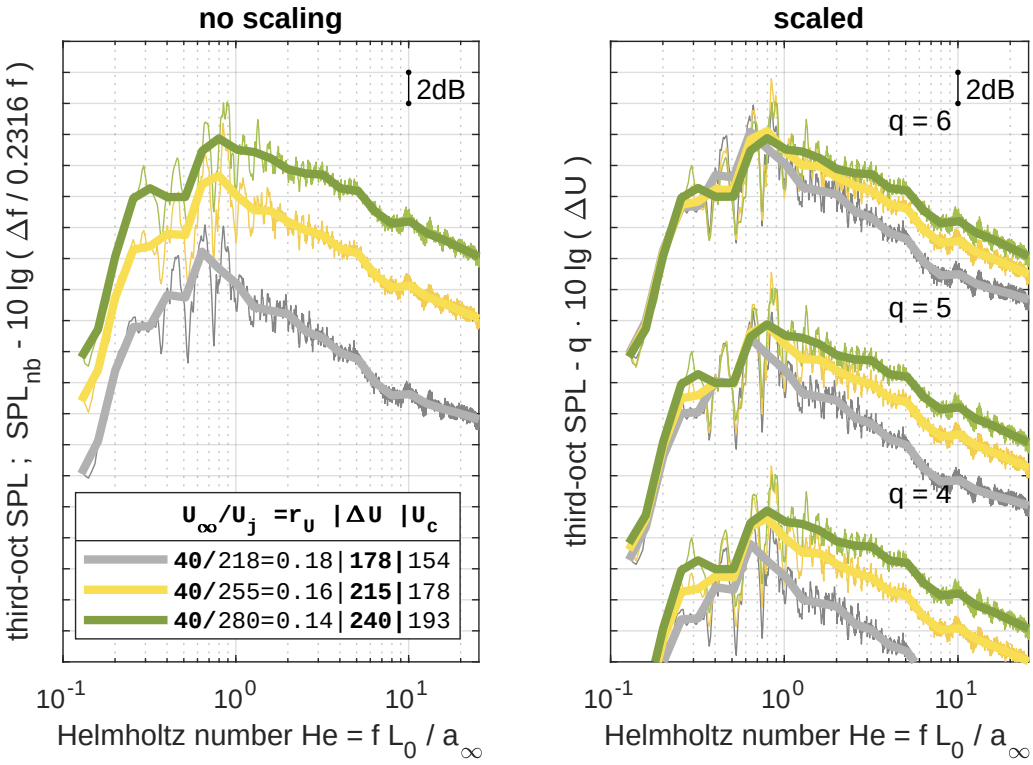

Fig. 15 **Same wind tunnel velocity** $U_\infty = 40\,\mathrm{m/s}$

Acknowledgments

Special thanks to the extended AWB and JExTRA test and analysis team, including H. Siller, W. Hage, and J.B. Mansoux, as well as A. Bassetti (DLR Berlin) and H. Demontis (ONERA).

The EU DJINN (Decrease Jet Installation Noise) project receives funding from the European Union's Horizon 2020 research and innovation programme under grant agreement No 861438. DJINN is a collaborative effort between CFD-Berlin (coordinator), Airbus SAS, Dassault Aviation, Safran Aircraft Engines, Rolls-Royce Deutschland, ONERA, DLR, University of Southampton, CERFACS, Imperial College London, von Karman Institute, CNRS, and Queen Mary University of London.

References

[1] Sengupta, G., "Analysis of jet-airframe interaction noise," *8th Aeroacoustics Conference*, Aeroacoustics Conferences, American Institute of Aeronautics and Astronautics, 1983. https://doi.org/10.2514/6.1983-783.

[2] Azarpeyvand, M., "An overview of jet noise research at the University of Bristol," *EU H2020 1st DJINN Conference: Industrially oriented jet noise reduction technologies*, 2021.

[3] Bridges, J., and Wernet, M., "Establishing Consensus Turbulence Statistics for Hot Subsonic Jets," *16th AIAA/CEAS Aeroacoustics Conference*, Aeroacoustics Conferences, American Institute of Aeronautics and Astronautics, 2010. https://doi.org/10.2514/6.2010-3751.

[4] Jente, C., and Delfs, J., "Velocity Scaling of Shear Layer Noise induced by cold Jet flow with co-flowing Flight stream," *25th AIAA/CEAS Aeroacoustics Conference*, Aeroacoustics Conferences, American Institute of Aeronautics and Astronautics, 2019. https://doi.org/10.2514/6.2019-2496.

[5] Tam, C., Viswanathan, K., Ahuja, K. K., and Panda, J., "The Sources of Jet Noise: Experimental Evidence," *13th AIAA/CEAS Aeroacoustics Conference (28th AIAA Aeroacoustics Conference)*, 2007. https://doi.org/10.2514/6.2007-3641.

[6] Tam, C. K. W., "A phenomenological approach to jet noise: the two-source model," *Philosophical Transactions of the Royal Society A: Mathematical, Physical and Engineering Sciences*, Vol. 377, No. 2159, 2019, p. 20190078. https://doi.org/10.1098/rsta.2019.0078.

[7] Witze, P. O., "Centerline Velocity Decay of Compressible Free Jets," *AIAA Journal*, Vol. 12, No. 4, 1974, pp. 417–418. https://doi.org/10.2514/3.49262.

[8] Abdel-Rahman, A., "A Review of Effects of Initial and Boundary Conditions on Turbulent Jets," *WSEAS Transactions on Fluid Mechanics*, Vol. 5, 2010.

[9] Pott-Pollenske, M., and Delfs, J., "Enhanced Capabilities of the Aeroacoustic Wind Tunnel Braunschweig," *14th AIAA/CEAS Aeroacoustics Conference (29th AIAA Aeroacoustics Conference)*, American Institute of Aeronautics and Astronautics, 2008. https://doi.org/10.2514/6.2008-2910.

[10] Viswanathan, K., "Mechanisms of Jet Noise Generation: Classical Theories and Recent Developments," *International Journal of Aeroacoustics*, Vol. 8, No. 4, 2009, pp. 355–407. https://doi.org/10.1260/147547209787548949.

[11] Microtech Gefell, "Condenser Measuring Microphone Cartridge Type MK 301," 2024, pp. 1–2. URL https://www.microtechgefell.de/datei/469/MK-301_TZdhG.pdf.

[12] Amiet, R. K., "Correction of open jet wind tunnel measurements for shear layer refraction," *2nd Aeroacoustics Conference*, 1975. https://doi.org/10.2514/6.1975-532.

[13] Bass, H. E., Sutherland, L. C., Zuckerwar, A. J., Blackstock, D. T., and Hester, D. M., "Atmospheric absorption of sound: Further developments," *Journal of the Acoustical Society of America*, Vol. 97, 1995, pp. 680–683. URL https://api.semanticscholar.org/CorpusID:123385958.

[14] "Acoustics - Attenuation of sound during propagation outdoors - Part 2: General method of calculation (ISO 9613-2:1996)," 1988, pp. 1–15. https://doi.org/10.31030/8139606.

[15] Michalke, A., and Michel, U., "Prediction of jet noise in flight from static tests," *Journal of Sound and Vibration*, Vol. 67, No. 3, 1979, pp. 341–367. https://doi.org/10.1016/0022-460X(79)90541-8.

[16] Harper-Bourne, M., "Jet Noise Measurements: Past and Present," *International Journal of Aeroacoustics*, Vol. 9, No. 4-5, 2010, pp. 559–588. https://doi.org/10.1260/1475-472X.9.4-5.559.

[17] Bridges, J., and Brown, C., "Validation of the Small Hot Jet Acoustic Rig for Aeroacoustic Research," *11th AIAA/CEAS Aeroacoustics Conference*, 2005. https://doi.org/10.2514/6.2005-2846.

[18] Brown, W. H., and Ahuja, K. K., "Jet and wing/flap interaction noise," *9th Aeroacoustics Conference*, 1984. https://doi.org/10.2514/6.1984-2362.

[19] Jente, C., "Jet-Flap Interaction Noise of Highly Integrated UHBR Turbofans," Ph.D. thesis, Technische Universität Braunschweig, 2023. Unpublished thesis.

[20] Davy, R., Mortain, F., Huet, M., and Garrec, T. L., "Installed jet noise source analysis by microphone array processing," *25th AIAA/CEAS Aeroacoustics Conference*, 2019. https://doi.org/10.2514/6.2019-2654.

[21] Lawrence, J., "Aeroacoustic interactions of installed subsonic round jets," Ph.D. thesis, University of Southampton, July 2014. URL https://eprints.soton.ac.uk/367059/.

[22] Amaral, F. R., Lebedev, A., and Jordan, P., "Experiments on installed jet noise," *AIAA AVIATION 2023 Forum*, 2023. https://doi.org/10.2514/6.2023-3830.

[23] Jente, C., Schmidt, J., Delfs, J., Rossignol, K.-S., Pott-Pollenske, M., and Siller, H. A., "Noise reduction potential of flow permeable materials for jet-flap interaction noise," *28th AIAA/CEAS Aeroacoustics 2022 Conference*, American Institute of Aeronautics and Astronautics, 2022. https://doi.org/10.2514/6.2022-3040.

[24] Faranosov, G., Kopiev, V., Ostrikov, N., and Kopiev, V. A., "The effect of pylon on the excess jet-flap interaction noise," *22nd AIAA/CEAS Aeroacoustics Conference*, 2016. https://doi.org/10.2514/6.2016-3043.

[25] Hunter, C., Thomas, R., Abdol-Hamid, K., Pao, S., Elmiligui, A., and Massey, S., "Computational Analysis of the Flow and Acoustic Effects of Jet-Pylon Interaction," *11th AIAA/CEAS Aeroacoustics Conference*, 2005. https://doi.org/10.2514/6.2005-3083.

[26] Viswanathan, K., and Lee, I. C., "Investigations of Azimuthal and Flight Effects on Noise from Realistic Turbofan Exhaust Geometries," *AIAA Journal*, Vol. 51, No. 6, 2013, pp. 1486–1505. https://doi.org/10.2514/1.J052138.

[27] Jente, C., Pott-Pollenske, M., Boenke, D., and Büscher, A., "Acoustic Similarity Modelling of a UHBR Jet Engine for the Investigation of Jet-Flap-Interaction Noise," *23rd AIAA/CEAS Aeroacoustics Conference*, AIAA AVIATION Forum, American Institute of Aeronautics and Astronautics, 2017. https://doi.org/10.2514/6.2017-3525.

[28] George, W. K., "The self-preservation of turbulent flows and its relation to initial conditions and coherent structures," *Advances in turbulence: Advances in turbulence*, edited by W. K. George and R. Arndt, Springer, Berlin, 1989, pp. 39–73.

[29] Delfs, J. W., "Vorlesung Basics of Aeroacoustics," , 2023. URL https://elib.dlr.de/202954/, complete Lecture notes "Basics of Aeroacoustics", held at Technische Universtät Braunschweig.

[30] Curle, N., and Lighthill, M. J., "The influence of solid boundaries upon aerodynamic sound," *Proceedings of the Royal Society of London. Series A. Mathematical and Physical Sciences*, Vol. 231, No. 1187, 1955, pp. 505–514. https://doi.org/10.1098/rspa.1955.0191.

[31] Ffowcs Williams, J. E., Hawkings, D. L., and Lighthill, M. J., "Sound generation by turbulence and surfaces in arbitrary motion," *Philosophical Transactions of the Royal Society of London. Series A, Mathematical and Physical Sciences*, Vol. 264, No. 1151, 1969, pp. 321–342. https://doi.org/10.1098/rsta.1969.0031.

[32] Lighthill, M. J., "On sound generated aerodynamically I. General theory," *Proceedings of the Royal Society of London. Series A. Mathematical and Physical Sciences*, Vol. 211, No. 1107, 1952, pp. 564–587. https://doi.org/10.1098/rspa.1952.0060.

[33] Jente, C., "Steady aerodynamics flow analysis for determining the necessary build space of an isolated jet shear layer," *EU H2020 1st DJINN Conference: Industrially oriented jet noise reduction technologies*, 2021. URL https://elib.dlr.de/146815/.

[34] Eisfeld, B., "Reynolds Stress Anisotropy in Self-Preserving Turbulent Shear Flows," Tech. rep., DLR, Juni 2017. URL https://elib.dlr.de/113887/.

[35] Huber, J., Pont, G., Jordan, P., and Roger, M., "Wavepacket Modelling of Jet-Flap Interaction Noise: from Laboratory to Full-Scale Aircraft," *Flow, Turbulence and Combustion*, 2024. https://doi.org/10.1007/s10494-023-00519-x.

[36] Jente, C., "Acoustic Mach number, jet Mach number or jet velocity: Choosing the optimal control property for jet noise experiments at different test rigs," *28th AIAA/CEAS Aeroacoustics 2022 Conference*, 2022. https://doi.org/10.2514/6.2022-2826.

[37] Fuchs, H., and Michel, U., "Experimental evidence of turbulent source coherence effecting jet noise," *4th Aeroacoustics Conference*, Aeroacoustics Conferences, American Institute of Aeronautics and Astronautics, 1977. https://doi.org/10.2514/6.1977-1348.

[38] Gaeta, R., and Ahuja, K., "Subtle Differences in Jet Noise Scaling with Narrow Band Spectra Compared to 1/3-Octave Band," *9th AIAA/CEAS Aeroacoustics Conference and Exhibit*, Aeroacoustics Conferences, American Institute of Aeronautics and Astronautics, 2003. https://doi.org/10.2514/6.2003-3124.